An ecologically based approach to terrestrial primary production

Grayson Badgley[1,2,+,*], Leander D.L. Anderegg[1,3,+], Joseph A. Berry[1], Christopher B. Field[2,4]

1. Department of Global Ecology, Carnegie Institution for Science, Stanford, CA, 94305
2. Department of Earth System Science, Stanford University, Stanford, CA, 94305
3. Department of Integrative Biology, University of California, Berkeley, CA, 94720
4. Woods Institute for the Environment, Stanford University, Stanford, CA, 94305

* badgley@stanford.edu

+ These authors contributed equally

Abstract

Terrestrial gross primary production (GPP) is both the largest and most uncertain flux within the global carbon cycle. Much of this uncertainty results from the fact that GPP is onerous to measure and is only reliably monitored at roughly 100 canopy-scale sites scattered across the globe. Sparsity of consistent GPP observations at the site-level translates into significant uncertainties in our understanding of the magnitude and spatial distribution of GPP at the global scale. We present a new, ecologically based approach for estimating GPP that takes advantage of the tendency for plants to capture only the amount of sunlight they are capable of efficiently using. Our approach uses a new remote sensing product that is sensitive to both the amount of light captured by plants and the efficiency with which plants use light for photosynthesis. The product is highly accurate in reproducing site-based GPP estimates, yet allows for simple calculation using data available globally for more than three decades. By precisely measuring the investment plants dedicate toward capturing and using light, we estimate global annual terrestrial photosynthesis to be 147 Pg C y^{-1} (95% credible interval 131-163 Pg C y^{-1}), which is intermediate between prevailing bottom-up machine learning and process-based GPP estimates and the top-down global constraint on GPP from oxygen isotopes. Furthermore, our approach enables the propagation and exploration of multiple sources of

uncertainty in our estimation of GPP, allowing for biological, statistical, and retrieval errors to be examined separately and further improvement in our understanding of global photosynthesis.

Introduction

Terrestrial photosynthesis (or gross primary production (GPP)) is responsible for fixing anywhere from 119 to 169 Pg C y^{-1}, making GPP both the largest and most uncertain component of the global carbon cycle [1]. Carbon fixed by photosynthesis in turn provides the basis for practically all life on land, providing a strong motivation for improving global estimates of GPP. It is especially important to understand how GPP might respond to global environmental change, as minor perturbations in terrestrial productivity have implications for global biodiversity, agriculture, and climate change [2, 3].

Quantifying terrestrial GPP is a complicated task, requiring precise measurements of the exchange of both energy and CO_2 between the land surface and the atmosphere. In these efforts, eddy covariance measurements of land surface CO_2 exchange have proved invaluable for estimating canopy and ecosystem scale photosynthesis and model validation [4, 5]. Despite their utility, eddy covariance measurements are limited in both time and space; individual flux sites measure CO_2 fluxes over approximately 1 km^2 and, in any given year, fewer than 100 sites operate globally, representing less than one millionth of total land area [6]. Such limitations especially hinder the validation of terrestrial ecosystem models, which operate globally at resolutions much greater than a single kilometer and need to integrate over processes with time constants from a fraction of a second to many years.

As a result, a host of semi-empirical upscaling approaches have emerged for translating site-level CO_2 fluxes to globally gridded photosynthesis estimates suitable for model benchmarking and development. Though many upscaling schemes exist, two approaches are by far the most widely applied: machine learning [7, 8] and remote sensing [9]. Both approaches leverage *in situ* fluxes to construct models relating site-level abiotic characteristics, plant traits, and meteorology to estimate photosynthesis beyond tower footprints. Upscaling allows for both the investigation of the drivers of global photosynthesis [10, 11] and for more extensive benchmarking of photosynthesis models by expanding the temporal and spatial availability of photosynthesis estimates [12, 13].

Yet any upscaling introduces uncertainties into GPP estimates, stemming both from model formulation and model inputs. Machine learning approaches, for example, provide the best possible constraint on GPP based on available data, but they functionally operate as black boxes. As a result, they make it difficult to diagnose the causes and consequences of uncertainty. Upscaling approaches are also limited by the availability of and the uncertainties contained within input datasets (e.g. meteorological data). Combined, these challenges limit the utility of upscaling for improving our process-based understanding of photosynthesis and determining the true value of global GPP. Presently, there exists a large and persistent disconnect between upscaled estimates of global GPP and higher estimates derived from top-down isotopic constraints [14].

Here, we report a novel approach for estimating global GPP that avoids many of the limitations posed by upscaling. The approach uses the near-infrared reflectance of vegetation (NIR_V), a reflectance-based index that is highly correlated with measured site-level GPP [15]. This correlation is a consequence of NIR_V integrating information on both canopy light capture and time-averaged light-use efficiency, which does not have a unique spectral signal, but is instead expressed through canopy structure. Plants endeavor to capture only the light they are capable of using; any strategy capturing more or less light would be inefficient and subject to the pressures of natural selection [16]. This optimality criterion, termed the resource balance or co-ordination hypothesis, means any measure of investment in light capture can serve as the basis for estimating GPP [17, 18]. Investment in light capture provides an index of canopy potential photosynthetic capacity, which should in turn closely match total resource availability. This approach has a long history in estimating net primary production (NPP) or biomass production, beginning with Monteith, who showed that a number of agricultural crops all converted sunlight into dry matter at a rate of approximately 1.4 g MJ^{-1} [19]. The light-use efficiency approach was subsequently extended to use satellite-based measures of light capture and applied to the global scale [20, 18]. But limitations in the available satellite indices meant that accurate GPP estimates required additional information on temperature and moisture levels. Because NIR_V integrates both light capture and light-use efficiency, it provides a uniquely useful index of investment in light capture and should be sufficient for estimating GPP without additional information on meteorological conditions. This avoids limitations in data availability and makes our approach capable of estimating GPP at high spatial resolution.

We present our results in three parts. First, we validate the NIR_V-GPP relationship at the site and global scale. Second, we extend the relationship to consider global GPP. Third, we evaluate some limitations in the global dataset of NIR_V and in the consistency of the NIR_V-GPP relationship.

Results

Using Bayesian hierarchical modeling, we found that NIR_V, combined with information on ecosystem type (deciduous, evergreen, and crop) explained 68% of the variation in annual GPP at 105 CO_2 monitoring sites (526 site-years that passed quality-control and data completeness requirements) and had an RMSE of 0.36 kg C m^{-2} y^{-1} (Fig. 1, see Methods). The approach required no additional information on meteorological conditions, such as site temperature or incoming radiation, indicating that NIR_V captures the effects of meteorology on GPP and supporting our interpretation of NIR_V as an integrator of whole-plant resource optimization (Fig. S1). Fewer inputs not only reduces uncertainty from input datasets, but also allows the NIR_V approach to be applied across a wide range of spatial and temporal scales. By contrast, existing remote sensing and machine learning based approaches for estimating GPP often require tens to hundreds of inputs. The NIR_V approach performed similarly well at the monthly time scale (Fig. 1, inset), explaining 56% of the observed variation in monthly GPP with an RMSE of 0.08 kg C m^{-2} mo^{-1}. The RMSE of NIR_V-based estimates of annual GPP was 42% lower than the RMSE of GPP fluxes calculated from BESS, a physiologically based land surface model, and was 57% higher than GPP estimates from FLUXCOM, a meteorological-based, statistical upscaling of FLUXNET GPP fluxes (Table S1).

For annual GPP, the most parsimonious model included just three ecosystem types, with a single intercept and separate NIR_V-GPP slopes for sites with i) evergreen, ii) deciduous, and iii) crop ecosystem types, as well as increasing variance in both residual error and site-level random intercepts as a function of NIR_V (Fig. S2). Further dividing ecosystem types resulted in minor model improvements, but an almost identical Deviance Information Criteria with more parameters, causing us to adopt the simpler three ecosystem type model (see Methods).

Applying this site-level scaling to globally resolved measurements of NIR_V, we estimated the median value of global annual GPP to be 147 Pg C y^{-1}, with a 95% credible interval of 131-163 Pg C y^{-1}. Our median GPP estimate is intermediate between estimates from spatial models and constraints from O_2 isotopes. FLUXCOM places annual GPP at 118 Pg C y^{-1}, while BESS puts mean global GPP at 122 Pg C y^{-1}. A meta-analysis of model-based annual GPP estimates ranged from 119 to 169 Pg C y^{-1} [1]. By contrast, O_2 isotopic measurements are consistent with global annual GPP in the range of 150 to 175 Pg C y^{-1} [14].

The spatial distribution of NIR_V-derived GPP was consistent with existing global GPP estimates, further validating our approach (Fig. 2). As expected, GPP was concentrated in the tropics and

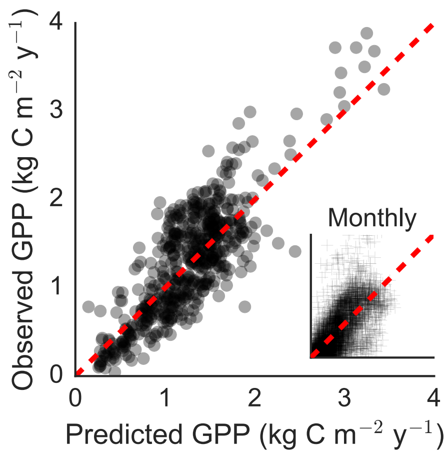

Figure 1. NIR_V explains a large portion of site-level GPP at both the monthly and annual timescale. Note the relatively large variation in monthly GPP estimates for low values of observed GPP, as compared to the near-zero intercept in the case of annual fluxes.

declined toward the poles. On a per biome basis, tropical forests contributed the most to global GPP, accounting for 31% of global GPP; FLUXCOM and BESS attribute 34% and 33% of GPP to tropical forests, respectively. Though lower in relative terms, NIR_V-derived GPP in tropical forests was 15% higher than both FLUXCOM and BESS GPP estimates in absolute terms. Instead, NIR_V assigned higher productivity to the midlatitudes, especially midlatitude mixed forests, grasslands, and shrub-dominated ecosystems (Fig. 2B; Table S2). One recent study that combined solar-induced chlorophyll fluorescence with a terrestrial ecosystem model found similar relative increases in extratropical GPP [21].

When compared on a per pixel basis, NIR_V was strongly linear with both FLUXCOM and BESS at the annual time scale, with R^2 exceeding 0.90 for both products and per pixel RMSE below 0.4 kg C m^{-2} y^{-1}, further emphasizing the robustness of NIR_V-derived GPP estimates (Fig. 3). This consistency is striking, given that our approach employed only two variables (NIR_V and ecosystem type), while both FLUXCOM and BESS require numerous environmental inputs. The comparison also emphasizes that NIR_V-derived GPP estimates are consistently higher than existing approaches, exceeding FLUXCOM GPP by a median value of 0.24 kg C m^{-2} y^{-1} and BESS GPP by 0.21 kg C m^{-2} y^{-1}. There are several possible reasons for this difference. On one hand, NIR_V might represent a theoretical upper bound of photosynthesis, prior to consideration of physiological effects (e.g., water or nutrient limitation), causing NIR_V-based GPP estimates to outpace physiologically based approaches. Alternatively, both BESS and FLUXCOM might systematically underestimate true GPP. Investigating the source of this discrepancy through more detailed comparisons of NIR_V

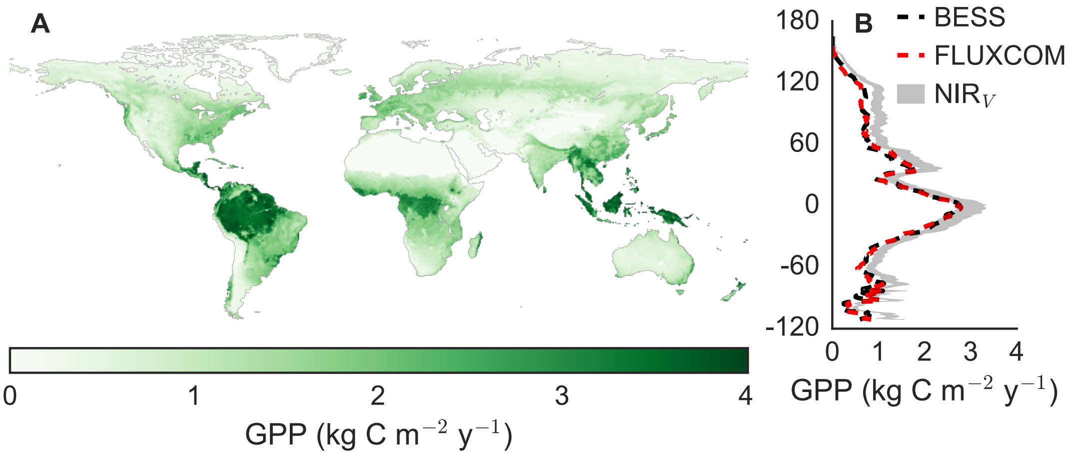

Figure 2. The A) global and B) latitudinal distribution of NIR$_\mathrm{V}$-derived GPP. Estimates represent the median of 1000 nearly independent upscalings of NIR$_\mathrm{V}$, while the full 95% credible range of GPP is shaded in grey for latitudinal estimates. The latitudinal distribution of annual GPP from FLUXCOM and BESS are shown for comparison.

against eddy covariance data and site-level modelling represents an important next step in using NIR$_\mathrm{V}$ to study photosynthesis at the global scale.

Model parsimony, combined with Bayesian estimation, allowed us to propagate three sources of uncertainty on a per pixel basis: statistical, variation in per ecosystem type scaling; site, deviation of a site intercept from the global per ecosystem type relationship; and residual, or otherwise unexplained errors. Median per pixel uncertainty was 0.20 kg C m^{-2} y^{-1} and total uncertainty, comprising all three sources of error, peaked in the tropics where total annual NIR$_\mathrm{V}$ was highest. In the worst case, the 95% credible interval of GPP exceeded 0.75 kg C m^{-2} y^{-1} in the Amazon basin and Indonesia (Fig. 4A). Given that tropical forests constitute the highest proportion of GPP (exceeding 30%), high uncertainty throughout the tropics significantly contributes to the overall uncertainty of global GPP estimates, regardless of approach.

Informative patterns emerge from examining the relative importance of statistical, site, and residual uncertainty on a per pixel basis; two examples of pixel-level uncertainties are shown in Fig. 4B. Outside of pixels with especially low NIR$_\mathrm{V}$, statistical uncertainty was always lowest, indicating minimal uncertainty in per ecosystem type scaling. On average, site uncertainty was always largest, meaning there was more uncertainty in the NIR$_\mathrm{V}$-GPP relationship from site to site than existed year to year (encompassed by residual uncertainty) at a single site. This indicates that either NIR$_\mathrm{V}$ or GPP estimates are not comparable across sites, which must be addressed by improving the accuracy of both measurements. The predominance of site-level uncertainty is a direct result of

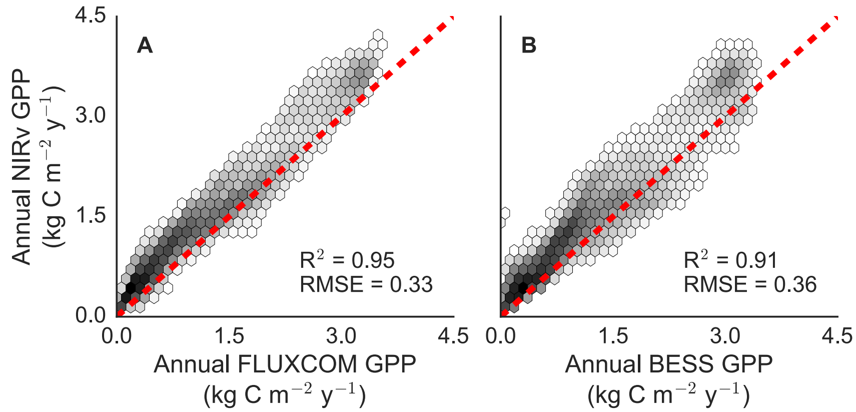

Figure 3. Upscaled $\mathrm{NIR_V}$-based estimates of annual GPP are linear with both A) FLUXCOM and B) BESS GPP estimates. $\mathrm{NIR_V}$-based estimates tend to be slightly higher than both FLUXCOM and BESS, though $\mathrm{NIR_V}$ has low a RMSE relative to both products. $\mathrm{NIR_V}$-based GPP estimate shown as the median case of 1000 nearly independent upscalings, see Methods.

considerable variation in site-level intercepts (Fig. S1). Site-to-site variability is randomly distributed, showing no relationship with site climate, thus highlighting retrieval errors (e.g., soil reflectance, clouds) as the likely cause of site-level uncertainty.

Discussion

$\mathrm{NIR_V}$ takes advantage of a globally consistent relationship between canopy structure and photosynthetic potential to provide an ecologically grounded approach for estimating GPP that combines a very simple formulation with excellent performance at validation sites (Figs. 1 and 3). As a result, $\mathrm{NIR_V}$ provides a novel means for upscaling GPP flux measurements that is largely independent of existing and widely used semi-empirical and process-based approaches. Finally, the $\mathrm{NIR_V}$ GPP approach achieves strong statistical performance while maintaining parsimony, allowing for i) an evolutionary and ecologically mechanistic interpretation of upscaling results, ii) straightforward analysis of uncertainty and how uncertainty is partitioned between model structure and inputs (Fig. 4), and iii) simple calculation.

Parsimony allows for a mechanistic interpretation of the $\mathrm{NIR_V}$-GPP relationship, in terms of how $\mathrm{NIR_V}$ and GPP jointly relate to canopy architecture and light capture. From a physical standpoint, $\mathrm{NIR_V}$ relates to variations in canopy leaf area and leaf display, serving as a useful index of the investment plants dedicate toward processing the light they capture [15]. Consistent with the resource balance hypothesis, plants tend to capture only as much light as they are capable of using

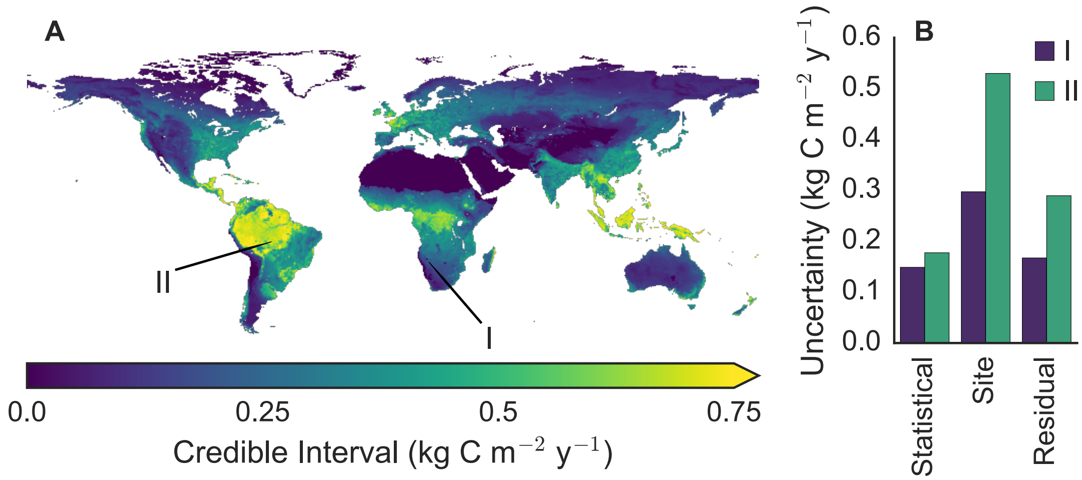

Figure 4. Bayesian hierarchical modeling allows for per pixel error estimation. A) Uncertainty in GPP peaks in the tropics (especially the Amazon and Indonesia), where the credible range of GPP exceed 0.75 kg C m^{-2} y^{-1}. B) Uncertainty can be evaluated on a per pixel basis, where site-level uncertainty is typically largest.

[17], helping explain the strength of the NIR_V-GPP relationship that otherwise has no strong physiological basis (Fig. 1). On an instantaneous basis, environmental factors like water, light, and temperature combine with leaf-level biochemical capacity to dictate the rate of photosynthesis; insights that are enshrined in leaf-level photosynthesis models [22]. The predictive ability of NIR_V, without the need for additional inputs like total incoming radiation, does not imply that environmental factors are irrelevant to photosynthesis, but rather that canopy architecture represents an emergent property that encapsulates the mechanistic controls of photosynthesis.

This mechanistic interpretation of the NIR_V-GPP relationship has implications for terrestrial photosynthesis models. We postulate that neglecting changes in canopy architecture within models can cause decoupling of light capture and canopy physiology. Models typically hold canopy architectural parameters (e.g., the ratio of sun and shade leaves) constant and instead vary leaf physiological parameters, like the maximum rate of carboxylation (V_{Cmax}). During periods of peak growth, for example, a model might underestimate light capture and compensate by arbitrarily adjusting V_{Cmax} to match GPP observations. This can result in V_{Cmax} becoming a model-dependent parameter, as opposed to a biologically interpretable measurement [12]. Future studies should consider combining measurements of NIR_V and V_{Cmax} to address this problem. These data would allow for independently fixing model V_{Cmax} using empirical data, while simultaneously varying canopy architecture as a function of observed NIR_V. Such an experiment would capitalize on the empirical NIR_V-GPP relationship to improve how process-based models represent both light capture and leaf physiology.

Another strength of the NIR_V approach is that it allows statistically valid error propagation (Fig. 4). More complicated approaches to estimating GPP make it difficult to accurately partition sources of error, especially model structural errors and errors due to input uncertainties. Minimizing upscaling complexity largely eliminates this problem. In particular, we were surprised by the predominance of site-level error; the NIR_V-GPP relationship always varied more from site to site than within a single site (Fig. 4B). This indicates that either the biology controlling the NIR_V-GPP relationship itself varies from site to site or that NIR_V and GPP measurements lack consistency across space. More simply, if the NIR_V-GPP relationship holds in general, deviations from this relationship should have either a biological or a methodological interpretation. The simplicity of our approach allows for the investigation of both possibilities.

As an example of measurement challenges, there is a stark disagreement in the NIR_V-GPP relationship at an eddy covariance site in French Guyana, GF-Guy. GPP fluxes at GF-Guy varied less than 20% month to month, while NIR_V varied by a factor of three (Fig. 5A). Assuming accurate GPP estimates, the divergence suggests errors in NIR_V observations at the site. We suspected cloud contamination, as remote sensing in the tropics is notoriously plagued by clouds degrading the accuracy of satellite measurements. To investigate this, we used the newly available MAIAC data product, which uses atmospheric modelling to remove aerosols, sub-pixel clouds, and other artifacts from MODIS satellite imagery [23]. The variability of NIR_V dramatically reduced with the MAIAC data (Fig. 5A). In fact, MAIAC-derived NIR_V had a smaller dynamic range than observed GPP, strongly indicating cloud contamination of the baseline MODIS dataset both at GF-Guy and, in all likelihood, throughout the tropics. Such contamination likely reduces our median global GPP estimate, making 147 Pg C y^{-1} a conservative estimate of global GPP. We expect that using MAIAC-derived NIR_V as the basis for estimating GPP would reduce site-level uncertainty and improve the accuracy of global GPP estimates. Unfortunately, such efforts will have to wait for a globally consistent MAIAC reprocessing of the full MODIS record.

Fundamental differences in plant physiology that govern the NIR_V and GPP relationship can also explain the predominance of site uncertainty. In this case, the simplicity of our approach leaves out potentially important biological determinants of productivity. Take for example the difference in C3 and C4 photosynthesis. C4 plants fix CO_2 more efficiently than C3 plants, which should cause a steeper slope in the NIR_V-GPP relationship, all else equal. When we examined a trio of Nebraskan eddy covariance towers that annually rotate between soy (C3) and corn (C4) crops, we found

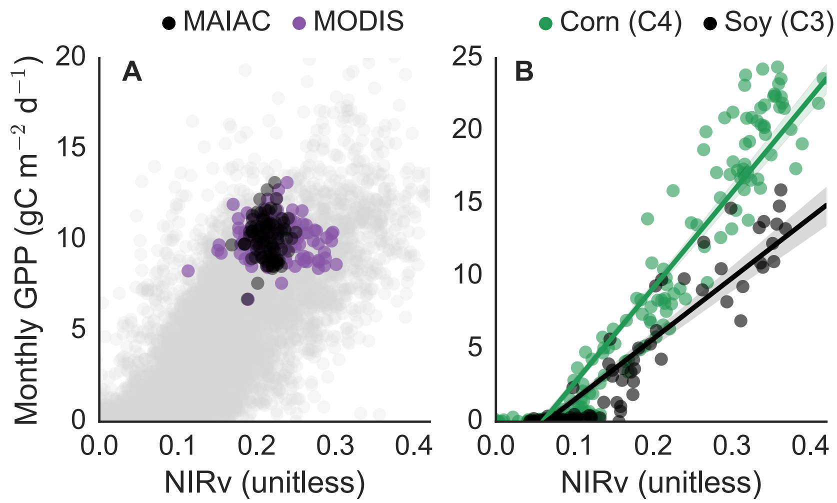

Figure 5. Parsimony allows for the investigation of sources of model uncertainty. A) Cloud contamination drives large monthly variations in MODIS collection 6 NIR_V that are not matched by variations in NIR_V. All monthly data from the FLUXNET2015 dataset shown in grey. B) Photosynthetic pathway predictably alters the NIR_V-GPP relationship, as C4 plants have greater efficiency.

significant differences in the NIR_V-GPP slope with crop type (Fig. 5B). As with cloud contamination, including information on the distribution of C3 and C4 vegetation across both wild and managed ecosystems would likely increase our global estimate of GPP, as C3 sites comprise the majority of data within the dataset used for calibration. This result further emphasizes the conservative nature of our 147 Pg C y^{-1} estimate of GPP. Apart from indicating that NIR_V-based GPP estimates could be further improved by incorporating a photosynthetic pathway parameter, this result also demonstrates how our ecologically grounded approach can be used to study plant physiology at the global scale.

The third advantage of the NIR_V approach is that NIR_V can be calculated from existing high-resolution and widely available satellite imagery. This makes NIR_V immediately available for benchmarking models at spatial and temporal scales relevant to land surface models, whether the model runs at 30 meters for a specific study site or spans the globe (Figs. 1 and 3). Our approach for estimating GPP from NIR_V could also be calculated for the full Landsat and MODIS records, as well as the 39 year record of the Advanced Very High Resolution Radiometer (AVHRR) series of sensors [24]. Long-term records that cover a range of climatic conditions are vital for benchmarking physiological models we hope to use in forecasting future ecological change. Finally, the ease of measuring NIR_V allows researchers to make inexpensive, canopy-scale spectral measurements that are directly comparable against satellite data, facilitating efforts to bridge spatial scales.

To conclude, we have developed a new, largely independent approach for estimating GPP that closely corresponds to existing best-in-class GPP estimates. Our robust handling of uncertainty demonstrates that current estimates of global GPP are likely too low and that the annual productivity of terrestrial ecosystems likely exceeds 147 Pg C y^{-1}, which more closely agrees with top-down, isotopically constrained estimates of GPP [14]. Further refinement of our NIR_V-based approach, through reducing input uncertainty and inclusion of additional physiological processes, will serve as a powerful new tool for validating terrestrial ecosystem models and improving our mechanistic understanding of the terrestrial carbon cycle.

Materials and Methods

Data

We compared NIR_V against monthly and annual GPP fluxes at 105 flux sites contained in the FLUXNET2015 Tier 1 dataset. For each site, we downloaded 500 meter, daily red (620-670nm) and near-infrared (NIR, 841-876nm) nadir-adjusted reflectances from MODIS collection MCD43A4.006 hosted on Google Earth Engine [25]. We calculated median NDVI and NIR for all scenes overlapping a 1km^2 circle around each fluxsite. Gaps were filled using linear interpolation. Finally, we multiplied median NDVI by NIR to calculate NIR_V and took the average of all daily NIR_V values for each month. We then combined monthly NIR_V estimates with monthly observations of GPP from the FLUXNET2015 dataset (variable name: GPP_VUT_MEAN). We required all site-months to have over 75% valid GPP observations and required site-years to have a minimum of 9 months of data. We gridded the MCD43A4.006 dataset to 0.5° to serve as the basis of our global upscaling.

In addition to the site-level comparisons, we evaluated NIR_V-based GPP estimates against two existing models of GPP: FLUXCOM, a machine learning approach for upscaling FLUXNET observations [8], and GPP estimates derived from the physiologically based land surface model, the Breathing Earth System Simulator (BESS), which has been extensively benchmarked against eddy covariance measurements of GPP [26, 27]. We used the mean ensemble of annual GPP_HB fluxes from the FLUXCOM CRUNCEPv6 product, accessed via the FLUXCOM website. For BESS, we used GPP estimates from BESS V1, obtained from the BESS website. Site-level RMSE values for FLUXCOM and BESS were derived from data provided by the authors [8, 27].

Calibration

We used Bayesian estimation to relate NIR_V and ecosystem type to GPP at both monthly and annual timescales. Bayesian estimation allows the propagation of uncertainty through hierarchical modeling, which allowed us to fit slope and intercept terms, as well as hierarchical variance terms capturing site-level random effects (random deviations from the global slope and intercept per site) and error variance [28]. We specified GPP as a linear function of NIR_V, with the best model (according to the Deviance Information Criteria; [28]) consisting of a single, near-zero intercept and differing slopes for evergreen, deciduous, and crop ecosystem types. The model included two additional terms: a random site-level intercept term and an error term that were both normally distributed with mean of 0 and variance exponentially related to NIR_V. See Supplementary Text 1 and Table S3 for a full description of the model structure, as well as alternative model structures tested. We used Markov chain Monte Carlo simulations (MCMC) implemented in JAGS [29] to sample the joint posterior distribution of fitted models, with initial diffuse priors for all parameters. We ran three parallel MCMC chains, evaluated chains for convergence, and thinned chains to remove within-chain autocorrelation, producing 1000 nearly independent draws from the posterior. We calculated site-level, median estimates of GPP and 95% credible intervals for model parameters based on the joint posterior distribution of the best model. We have posted the GPP calibration code to www.github.com/badgley/nirv-global.

Upscaling

We produced global annual estimates of GPP with the best annual NIR_V model, using all 1000 draws from the joint model posterior to calculate GPP for all land pixels from 2005 to 2015. For each posterior draw, we calculated GPP of every pixel based on the per-biome scaling parameter plus randomly sampled site-level and residual error based on the site and residual variance parameter estimates for that draw. Using the site-level model for our global upscaling captures correlations between parameter estimates (scaling slope and site-level variance estimates were often correlated), resulting in GPP estimates that appropriately represent statistical, site, and residual uncertainty from the full joint posterior distribution of the model. We present the median and 95% credible intervals from the distribution of the upscaled GPP estimates. We excluded pixels with a landcover classification of “barren”.

Acknowledgments

We thank J. Johnson and Y. Shiga for the many conversations that clarified our thinking, as well as Y. Ryu and M. Whelan, whom reviewed earlier drafts of this work. G. Tramontana and C. Jiang kindly provided site-level GPP fluxes for comparison. B. Peng shared the C3/C4 crop rotation data. Funds from a NASA Earth and Space Science fellowship (G.B.), a NOAA Climate and Global Change fellowship, and NSF Postdoctoral Research Fellowship Grant No. DBI-1711243 (L.D.L.A) supported this research. Any opinions, findings, and conclusions or recommendations expressed in this material are those of the author(s) and do not necessarily reflect the views of the National Science Foundation. This work used eddy covariance data acquired and shared by the FLUXNET community, including these networks: AmeriFlux, AfriFlux, AsiaFlux, CarboAfrica, CarboEuropeIP, CarboItaly, CarboMont, ChinaFlux, Fluxnet-Canada, GreenGrass, ICOS, KoFlux, LBA, NECC, OzFlux-TERN, TCOS-Siberia, and USCCC. The ERA-Interim reanalysis data are provided by ECMWF and processed by LSCE. The FLUXNET eddy covariance data processing and harmonization was carried out by the European Fluxes Database Cluster, AmeriFlux Management Project, and Fluxdata project of FLUXNET, with the support of CDIAC and ICOS Ecosystem Thematic Center, and the OzFlux, ChinaFlux and AsiaFlux offices.

References

[1] A. Anav, P. Friedlingstein, C. Beer, P. Ciais, A. Harper, C. Jones, G. Murray-Tortarolo, D. Papale, N. C. Parazoo, P. Peylin, et al. “Spatiotemporal patterns of terrestrial gross primary production: A review”. *Reviews of Geophysics* 53.3 (2015), pp. 785–818.

[2] J. Rockström, W. Steffen, K. Noone, Å. Persson, F. S. Chapin III, E. F. Lambin, T. M. Lenton, M. Scheffer, C. Folke, H. J. Schellnhuber, et al. “A safe operating space for humanity”. *Nature* 461.7263 (2009), pp. 472–475.

[3] S. W. Running. “A measurable planetary boundary for the biosphere”. *Science* 337.6101 (2012), pp. 1458–1459.

[4] D. Baldocchi, E. Falge, L. Gu, R. Olson, D. Hollinger, S. Running, P. Anthoni, C. Bernhofer, K. Davis, R. Evans, et al. “FLUXNET: A new tool to study the temporal and spatial variability of ecosystem-scale carbon dioxide, water vapor, and energy flux densities”. *Bulletin of the American Meteorological Society* 82.11 (2001), pp. 2415–2434.

[5] D. Baldocchi. "'Breathing' of the terrestrial biosphere: lessons learned from a global network of carbon dioxide flux measurement systems". *Australian Journal of Botany* 56.1 (2008), pp. 1–26.

[6] J. Kumar, F. M. Hoffman, W. W. Hargrove, and N. Collier. "Understanding the representativeness of FLUXNET for upscaling carbon flux from eddy covariance measurements". *Earth System Science Data Discussions* (Aug. 2016).

[7] C. Beer, M. Reichstein, E. Tomelleri, P. Ciais, M. Jung, N. Carvalhais, C. Rödenbeck, M. A. Arain, D. Baldocchi, G. B. Bonan, et al. "Terrestrial gross carbon dioxide uptake: global distribution and covariation with climate". *Science* (2010), p. 1184984.

[8] G. Tramontana, M. Jung, C. R. Schwalm, K. Ichii, G. Camps-Valls, B. Ráduly, M. Reichstein, M. A. Arain, A. Cescatti, G. Kiely, et al. "Predicting carbon dioxide and energy fluxes across global FLUXNET sites with regression algorithms". *Biogeosciences* (2016).

[9] S. W. Running, R. R. Nemani, F. A. Heinsch, M. Zhao, M. Reeves, and H. Hashimoto. "A continuous satellite-derived measure of global terrestrial primary production". *BioScience* 54.6 (2004), pp. 547–560.

[10] M. Jung, M. Reichstein, C. R. Schwalm, C. Huntingford, S. Sitch, A. Ahlström, A. Arneth, G. Camps-Valls, P. Ciais, P. Friedlingstein, et al. "Compensatory water effects link yearly global land CO 2 sink changes to temperature". *Nature* 541.7638 (2017), pp. 516–520.

[11] M. Zhao and S. W. Running. "Drought-induced reduction in global terrestrial net primary production from 2000 through 2009". *Science* 329.5994 (2010), pp. 940–943.

[12] G. B. Bonan, P. J. Lawrence, K. W. Oleson, S. Levis, M. Jung, M. Reichstein, D. M. Lawrence, and S. C. Swenson. "Improving canopy processes in the Community Land Model version 4 (CLM4) using global flux fields empirically inferred from FLUXNET data". *Journal of Geophysical Research: Biogeosciences* 116.G2 (2011).

[13] M. Williams, A. Richardson, M. Reichstein, P. Stoy, P. Peylin, H. Verbeeck, N. Carvalhais, M. Jung, D. Hollinger, J. Kattge, et al. "Improving land surface models with FLUXNET data". *Biogeosciences* 6.7 (2009), pp. 1341–1359.

[14] L. R. Welp, R. F. Keeling, H. A. Meijer, A. F. Bollenbacher, S. C. Piper, K. Yoshimura, R. J. Francey, C. E. Allison, and M. Wahlen. "Interannual variability in the oxygen isotopes of atmospheric CO 2 driven by El Niño". *Nature* 477.7366 (2011), pp. 579–582.

[15] G. Badgley, C. B. Field, and J. A. Berry. "Canopy near-infrared reflectance and terrestrial photosynthesis." *Science Advances* 3.3 (2017), e1602244.

[16] A. J. Bloom, F. S. Chapin, and H. A. Mooney. "Resource limitation in plants - an economic analogy". *Annual Review of Ecology and Systematics* 16 (1985), pp. 363–392.

[17] C. B. Field. "Ecological scaling of carbon gain to stress and resource". In: *Response of Plants to Multiple Stresses*. Academic Press San Diego, 1991, pp. 35–65.

[18] C. B. Field, J. T. Randerson, and C. M. Malmström. "Global net primary production: combining ecology and remote sensing". *Remote sensing of Environment* 51.1 (1995), pp. 74–88.

[19] J. L. Monteith. "Climate and the efficiency of crop production in Britain". *Philosophical Transactions of the Royal Society London B* 281.980 (1977), pp. 277–294.

[20] C. S. Potter, J. T. Randerson, C. B. Field, P. A. Matson, P. M. Vitousek, H. A. Mooney, and S. A. Klooster. "Terrestrial ecosystem production: a process model based on global satellite and surface data". *Global Biogeochemical Cycles* 7.4 (1993), pp. 811–841.

[21] A. J. Norton, P. J. Rayner, E. N. Koffi, M. Scholze, J. D. Silver, and Y.-P. Wang. "Estimating global gross primary productivity using chlorophyll fluorescence and a data assimilation system with the BETHY-SCOPE model". *Biogeosciences Discussions* 2018 (2018), pp. 1–40.

[22] G. D. Farquhar, S. von Caemmerer, and J. A. Berry. "A biochemical model of photosynthetic CO2 assimilation in leaves of C3 species". *Planta* 149.1 (1980), pp. 78–90.

[23] A. Lyapustin, J. Martonchik, Y. Wang, I. Laszlo, and S. Korkin. "Multiangle implementation of atmospheric correction (MAIAC): 1. Radiative transfer basis and look-up tables". *Journal of Geophysical Research: Atmospheres* 116.D3 (2011).

[24] C. J. Tucker, J. E. Pinzon, M. E. Brown, D. A. Slayback, E. W. Pak, R. Mahoney, E. F. Vermote, and N. El Saleous. "An extended AVHRR 8-km NDVI dataset compatible with MODIS and SPOT vegetation NDVI data". *International Journal of Remote Sensing* 26.20 (2005), pp. 4485–4498.

[25] C. Schaaf and Z. Wang. "MCD43A4 MODIS/Terra+ Aqua BRDF/Albedo Nadir BRDF Adjusted RefDaily L3 Global 500 m V006". *NASA EOSDIS Land Processes DAAC* (2015).

[26] Y. Ryu, D. D. Baldocchi, H. Kobayashi, C. van Ingen, J. Li, T. A. Black, J. Beringer, E. Van Gorsel, A. Knohl, B. E. Law, et al. "Integration of MODIS land and atmosphere products with a coupled-process model to estimate gross primary productivity and evapotranspiration from 1 km to global scales". *Global Biogeochemical Cycles* 25.4 (2011).

[27] C. Jiang and Y. Ryu. "Multi-scale evaluation of global gross primary productivity and evapotranspiration products derived from Breathing Earth System Simulator (BESS)". *Remote Sensing of Environment* 186 (2016), pp. 528–547.

[28] A. Gelman, J. B. Carlin, H. S. Stern, and D. B. Rubin. *Bayesian data analysis*. Chapman and Hall/CRC, 1995.

[29] M. Plummer. *JAGS: A program for analysis of Bayesian graphical models using Gibbs sampling*. 2003.

Supplementary Information for

NIRv-GPP Supplement

Grayson Badgley, Leander D.L. Anderegg, Joseph A. Berry, Christopher B. Field

Grayson Badgley
E-mail: badgley@stanford.edu

This PDF file includes:

Supplementary text
Figs. S1 to S2
Tables S1 to S4
References for SI reference citations

Supporting Information Text

Supplementary Text 1: Bayesian Modeling

We used Bayesian estimation to fit linear mixed effects models relating GPP to NIR_V. For the sake of simplicity, we modeled annual or monthly GPP as a linear function of NIR_V, and explored a variety of model structures allowing both slopes and intercepts to differ by land cover class or leaf habit, with random site-level effects. Preliminary model selection suggested that site-level random slope and intercept terms were not needed for the annual model, but were needed for monthly model. For the annual model, we explored a variety of fixed effects structures, as well as a number of variance functions (for residual variation and site-level intercepts). See Table S3 for list of annual models explored and their associated Deviance Information Criteria scores (DIC). All error functions assumed normally distributed errors and similar functional forms for residual error and site random intercepts, but with residual errors being a function of observed annual NIR_V and site random intercepts a function of site mean annual NIR_V, treating true NIR_V as a latent variable) are easily implemented in this modeling framework, though we present the simplest defensible case for the sake of illustration and intuitive upscaling. We produced global annual estimates of GPP using the posterior distribution of the best annual NIR_V model (bolded in Table S3).

Open Source Software

Python. All analyses, with the exception of the Bayesian modeling, were performed using the Python programming language. We processed netCDF files and tabular data using xarray (1), pandas (2), and numpy (3). We used matplotlib (4) and seaborn (5) for visualization, and Jupyter notebooks for organizing analyses (6).

R. We ran all Bayesian modeling in the R programming environment (7), making using of the "r2jags" package (8) to interface with JAGS, a Bayesian modeling software package (9).

GPP Product	RMSE (kg C m^{-2} y^{-1})
NIR_V	0.36
BESS	0.55
FLUXCOM	0.20

Table S1. Site-level RMSE of 106 FLUXNET2015 site for each of the three GPP products considered in this study.

	NIR_V		BESS		FLUXCOM	
	GPP (Pg C y^{-1})	Fraction (%)	GPP (Pg C y^{-1})	Fraction (%)	GPP (Pg C y^{-1})	Fraction (%)
Evergreen Broadleaf forest	46.74	31.70	40.18	33.66	40.48	34.21
Mixed forest	16.28	11.04	10.61	8.89	11.24	9.50
Woody savannas	15.00	10.17	15.21	12.74	14.12	11.94
Savannas	14.79	10.03	13.08	10.96	13.00	10.99
Croplands	13.82	9.38	10.42	8.73	10.48	8.86
Grasslands	12.11	8.21	9.25	7.75	7.84	6.63
Open shrublands	10.89	7.39	6.01	5.04	6.23	5.27
Cropland/Natural vegetation mosaic	9.74	6.61	8.98	7.52	8.64	7.30
Evergreen Needleleaf forest	4.12	2.80	2.69	2.26	2.87	2.42
Other	1.97	1.34	1.69	1.41	1.55	1.31
Deciduous Broadleaf forest	1.96	1.33	1.24	1.04	1.87	1.58

Table S2. Per biome distribution GPP for NIR_V, BESS, and FLUXCOM global GPP products.

Model Structure	Variance Structure	# fixed params	DIC
GPP intercept + NIR_V:leaf habit	a	4	7142.393
GPP intercept + NIR_V:leaf habit	$a + b \cdot NIR_V$	4	7134.997
GPP intercept + NIR_V:leaf habit	$a + e^{zNIR_V \cdot b}$	4	7146.137
GPP intercept + NIR_V:leaf habit	$a + b \cdot e^{zNIR_V}$	4	7150.204
GPP intercept + NIR_V:leaf habit	$a + NIR_V^b$	4	7150.299
GPP intercept + NIR_V:leaf habit	$\boldsymbol{NIR_V^b}$	**4**	**7104.392***
GPP intercept + NIR_V:leaf habit	$a + b * NIR_V^2$	4	7127.383
GPP intercept:leaf habit + slope:leaf habit	NIR_V^b	6	7106.333
GPP intercept:land cover + slope:land cover	NIR_V^b	22	7106.601
GPP intercept + slope:land cover	NIR_V^b	12	7111.44

Table S3. Potential annual models tested, including various fixed structures and various variance formulations. Variance functions were fit for the standard deviation of both the residual error and the site-level random intercept, where NIR_V is annual observed NIR_V for the residual error and the site mean annual NIR_V for the site random intercept. "$zNIR_V$" indicates that NIR_V values were z-score standardized.

Site	Latitude	Longitude	Years	Reference
AR-Vir	-28.2395	-56.1886	2009–2012	(10)
AT-Neu	47.1167	11.3175	2002–2012	(11)
AU-ASM	-22.283	133.249	2010–2013	(12)
AU-Ade	-13.0769	131.1178	2007–2009	(13)
AU-Cpr	-34.0021	140.5891	2010–2013	(14)
AU-Cum	-33.6133	150.7225	2012–2013	(14)
AU-DaP	-14.0633	131.3181	2008–2013	(13)
AU-DaS	-14.1593	131.3881	2008–2013	(13)
AU-Dry	-15.2588	132.3706	2008–2013	(13)
AU-Emr	-23.8587	148.4746	2011–2013	(15)
AU-Fog	-12.5452	131.3072	2006–2008	(13)
AU-GWW	-30.1913	120.6541	2013–2014	(16)
AU-RDF	-14.5636	132.4776	2011–2013	(13)
AU-Rig	-36.6499	145.5759	2011–2013	(13)
AU-Tum	-35.6566	148.1517	2001–2013	(17)
AU-Whr	-36.6732	145.0294	2011–2013	(14)
BE-Bra	51.3092	4.5206	2000–2013	(18)
BE-Lon	50.5516	4.7461	2004–2014	(19)
BE-Vie	50.3051	5.9981	2000–2014	(20)
BR-Sa3	-3.018	-54.9714	2000–2004	(21)
CA-NS1	55.8792	-98.4839	2002–2005	(22)
CA-NS2	55.9058	-98.5247	2001-2005	(22)
CA-NS3	55.9117	-98.3822	2001–2005	(22)
CA-NS4	55.9117	-98.3822	2002–2005	(22)
CA-NS5	55.8631	-98.485	2001–2005	(22)
CA-NS6	55.9167	-98.9644	2001–2005	(22)
CA-NS7	56.6358	-99.9483	2002–2005	(22)
CA-Qfo	49.6925	-74.3421	2003–2010	(23)
CH-Cha	47.2102	8.4104	2006–2012	(24)
CH-Fru	47.1158	8.5378	2006–2012	(24)
CH-Oe1	47.2858	7.7319	2002–2008	(25)
CN-Cha	42.4025	128.0958	2003–2005	(26)
CN-Cng	44.5934	123.5092	2007–2010	(27)
CN-Dan	30.4978	91.0664	2004–2005	(28)
CN-Din	23.1733	112.5361	2003–2005	(28)
CN-Du2	42.0467	116.2836	2006–2008	(29)
CN-Ha2	37.6086	101.3269	2003–2005	(30)
CN-HaM	37.37	101.18	2002–2004	(31)
CN-Qia	26.7414	115.0581	2003–2005	(28)
CN-Sw2	41.7902	111.8971	2010–2012	(32)
DE-Akm	53.8662	13.6834	2009–2014	http://www.fluxdata.org:8080/sitepages/siteInfo.aspx?DE-Akm
DE-Gri	50.9495	13.5125	2004–2014	(33)
DE-Hai	51.0792	10.453	2000–2012	(34)
DE-Kli	50.8929	13.5225	2004–2014	(35)
DE-Obe	50.7836	13.7196	2008–2014	(36)
DE-RuS	50.8659	6.4472	2011–2014	(37)
DE-Sfn	47.8064	11.3275	2012-2014	(38)
DE-Spw	51.8923	14.0337	2010–2014	http://www.fluxdata.org:8080/sitepages/siteInfo.aspx?DE-spw
DE-Tha	50.9636	13.5669	2000–2014	(39)
DK-Sor	55.4859	11.6446	2000–2012	(40)
ES-LgS	37.0979	-2.9658	2007–2009	(41)
FI-Hyy	61.8475	24.295	2000–2014	(42)
FR-Gri	48.8442	1.9519	2004–2013	(43)
FR-Fon	48.4764	2.7801	2005-2014	(44)
FR-Pue	43.7414	3.5958	2000–2013	(45)
GF-Guy	5.2788	-52.9249	2004–2012	(46)
IT-BCi	40.5238	14.9574	2004-2014	(47)
IT-CA1	42.3804	12.0266	2011–2013	(48)
IT-CA2	42.3772	12.026	2011–2013	(48)

IT-CA3	42.38	12.0222	2011–2013	(48)
IT-Cp2	41.7043	12.3573	2012–2013	(49)
IT-Isp	45.8126	8.6336	2013–2014	(50)
IT-Lav	45.9562	11.2813	2003–2012	(51)
IT-Noe	40.6061	8.1515	2004–2012	(52)
IT-PT1	45.2009	9.061	2002–2004	(53)
IT-Ren	46.5869	11.4337	2000–2013	(54)
IT-Ro1	42.4081	11.93	2000–2008	(55)
IT-Ro2	42.3903	11.9209	2002–2012	(56)
IT-SR2	43.732	10.291	2013–2014	(57)
IT-SRo	43.7279	10.2844	2000–2012	(57)
IT-Tor	45.8444	7.5781	2008–2013	(58)
JP-MBF	44.3869	142.3186	2003–2005	(59)
JP-SMF	35.2617	137.0788	2002–2006	(59)
NL-Hor	52.2404	5.0713	2004–2011	(60)
NL-Loo	52.1666	5.7436	1996–2013	(61)
RU-Fyo	56.4615	32.9221	2000–2013	(62)
SD-Dem	13.2829	30.4783	2005–2009	(63)
US-AR1	36.4267	-99.42	2009–2012	(64)
US-AR2	36.6358	-99.5975	2009–2012	(64)
US-ARM	36.6058	-97.4888	2003–2012	(65)
US-Blo	38.8953	-120.633	2000–2007	(66)
US-Ha1	42.5378	-72.1715	2000–2012	(67)
US-Los	46.0827	-89.9792	2000–2014	(68)
US-MMS	39.3232	-86.4131	2000–2014	(69)
US-Me2	44.4523	-121.5574	2002-2014	(70)
US-Me6	44.3233	-121.608	2010–2012	(71)
US-Myb	38.0498	-121.765	2011–2014	(72)
US-Ne1	41.1651	-96.4766	2001–2013	(73)
US-Ne2	41.1649	-96.4701	2001–2013	(73)
US-Ne3	41.1797	-96.4397	2001–2013	(73)
US-NR1	40.0329	-105.5464	1998-2014	(74)
US-PFa	45.9459	-90.2723	1995-2014	(75)
US-SRG	31.7894	-110.8277	2008-2014	(76)
US-SRM	31.8214	-110.866	2004–2014	(77)
US-Syv	46.242	-89.3477	2001–2014	(78)
US-Ton	38.4316	-120.966	2001–2014	(79)
US-Twt	38.1087	-121.6530	2009-2014	(80)
US-UMB	45.5598	-84.7138	2000-2014	(81)
US-UMd	45.5625	-84.6975	2007–2014	(82)
US-Var	38.4133	-120.951	2000–2014	(83)
US-WCr	45.8059	-90.0799	2000–2014	(84)
US-Whs	31.7438	-110.052	2007–2014	(77)
US-Wkg	31.7365	-109.942	2004–2014	(85)
ZA-Kru	-25.0197	31.4969	2000–2010	(86)
ZM-Mon	-15.4378	23.2528	2007–2009	(87)

Table S4. The FLUXNET2015 sites used in this study.

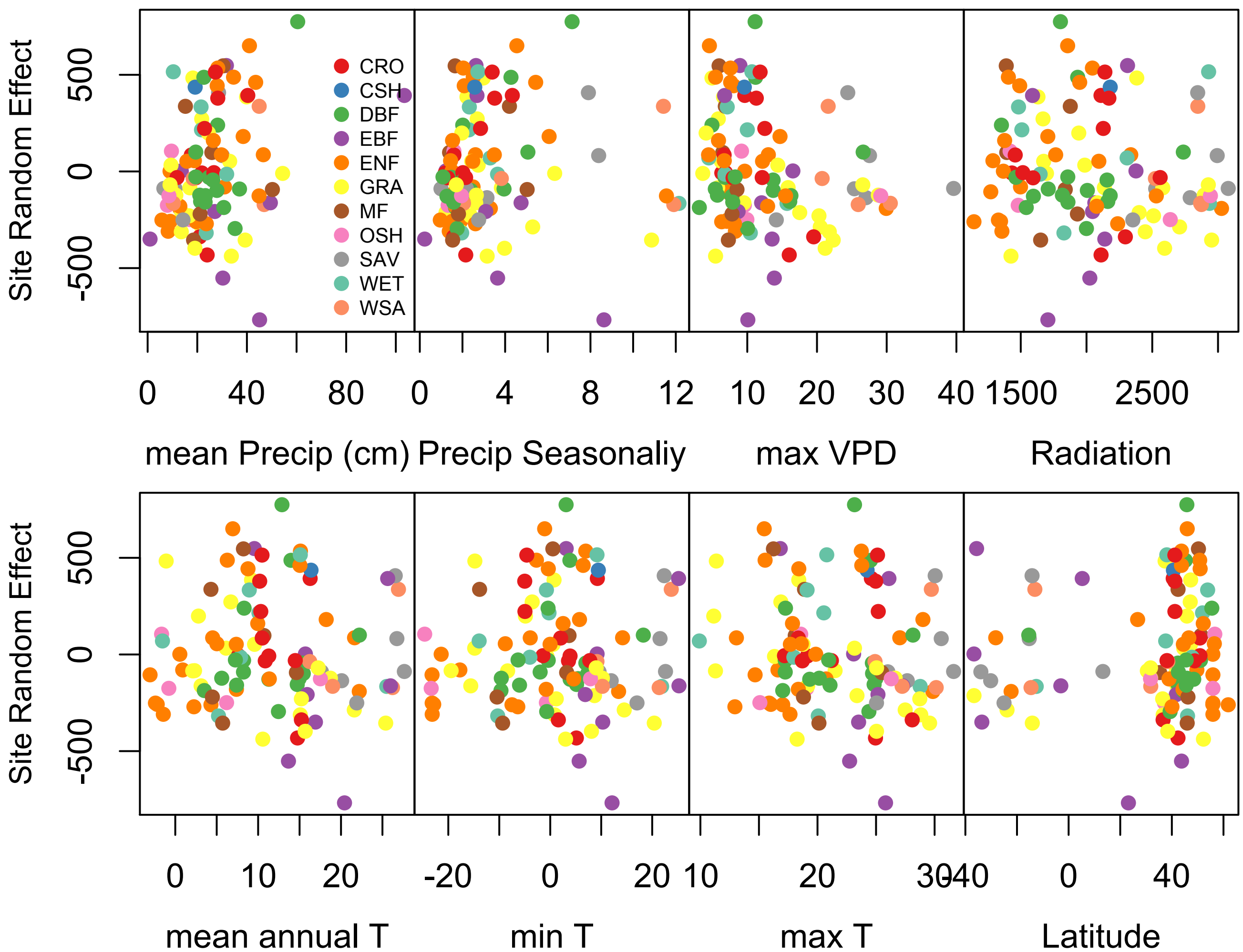

Fig. S1. Residuals of the final Bayesian model plotted against various, site-level meteorlogical data show no coherent patterns, demonstrating that NIR_V already captures the effects many environmental factors exert on GPP at the annual timescale.

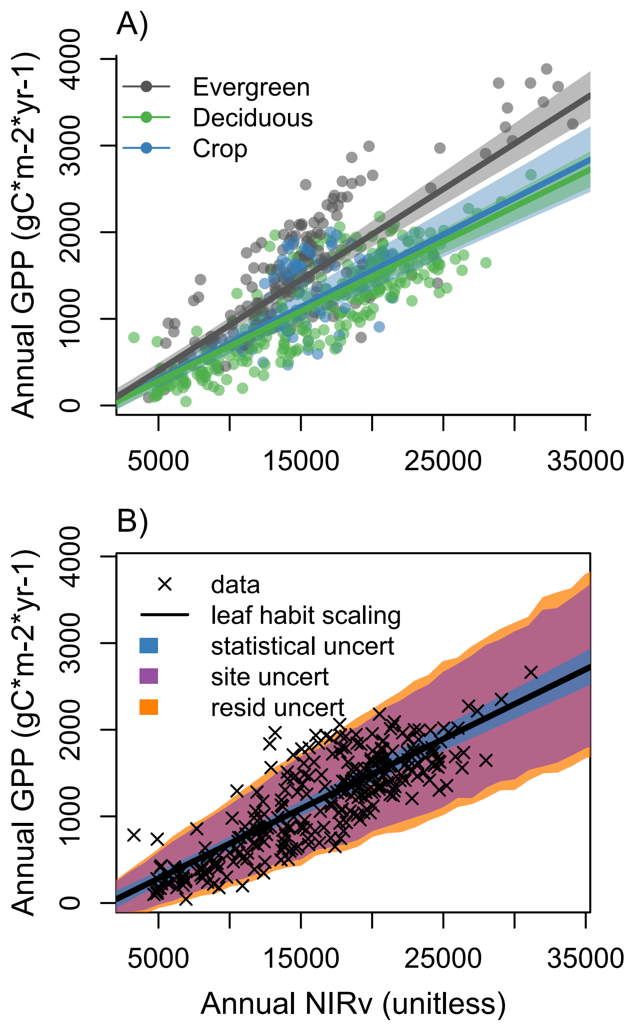

Fig. S2. Depiction of A) the final model formulation and B) the structure of model uncertainties. Each leaf habit shared an intercept of 0, but had slightly different NIR_V to GPP slope. Errors increased exponentially with observed NIR_V, with site-level uncertainty having the largest relative contribution to total per pixel error.

References

1. Hoyer S, Hamman J (2017) xarray: N-D labeled arrays and datasets in Python. *Journal of Open Research Software* 5(1).
2. McKinney W, , et al. (2010) Data structures for statistical computing in python in *Proceedings of the 9th Python in Science Conference*. (Austin, TX), Vol. 445, pp. 51–56.
3. Walt Svd, Colbert SC, Varoquaux G (2011) The numpy array: a structure for efficient numerical computation. *Computing in Science & Engineering* 13(2):22–30.
4. Hunter JD (2007) Matplotlib: A 2d graphics environment. *Computing in science & engineering* 9(3):90–95.
5. Waskom M, et al. (2014) seaborn: v0.5.0 (november 2014).
6. Kluyver T, et al. (2016) Jupyter notebooks – a publishing format for reproducible computational workflows in *Positioning and Power in Academic Publishing: Players, Agents and Agendas*, eds. Loizides F, Schmidt B. (IOS Press), pp. 87 – 90.
7. Team RC (2014) R: A language and environment for statistical computing. r foundation for statistical computing, vienna, austria. 2013.
8. Su YS, Yajima M (2015) R2jags: Using r to run 'jags'. *R package version 0.5-7*.
9. Plummer M (2013) rjags: Bayesian graphical models using mcmc. *R package version* 3(10).
10. Posse G, Lewczuk N, Richter K, Cristiano P (2016) Carbon and water vapor balance in a subtropical pine plantation. *iForest-Biogeosciences and Forestry* 9(5):736.
11. Wohlfahrt G, et al. (2008) Seasonal and inter-annual variability of the net ecosystem co2 exchange of a temperate mountain grassland: Effects of weather and management. *Journal of Geophysical Research: Atmospheres* 113(D8).
12. Eamus D, et al. (2013) Carbon and water fluxes in an arid-zone acacia savanna woodland: An analyses of seasonal patterns and responses to rainfall events. *Agricultural and Forest Meteorology* 182:225–238.
13. Beringer J, Hutley LB, Hacker JM, Neininger B, , et al. (2011) Patterns and processes of carbon, water and energy cycles across northern australian landscapes: From point to region. *Agricultural and Forest Meteorology* 151(11):1409–1416.
14. Karan M, et al. (2016) The australian supersite network: A continental, long-term terrestrial ecosystem observatory. *Science of the Total Environment* 568:1263–1274.
15. Schroder I (2014) Arcturus emerald ozflux tower site. *OzFlux: Australian and New Zealand Flux Research and Monitoring, hdl* 102(100):14249.
16. Prober SM, et al. (2012) Facilitating adaptation of biodiversity to climate change: a conceptual framework applied to the world's largest mediterranean-climate woodland. *Climatic Change* 110(1-2):227–248.
17. Leuning R, Cleugh HA, Zegelin SJ, Hughes D (2005) Carbon and water fluxes over a temperate eucalyptus forest and a tropical wet/dry savanna in australia: measurements and comparison with modis remote sensing estimates. *Agricultural and Forest Meteorology* 129(3-4):151–173.
18. Carrara A, et al. (2003) Net ecosystem co2 exchange of mixed forest in belgium over 5 years. *Agricultural and Forest Meteorology* 119(3-4):209–227.
19. Moureaux C, Debacq A, Bodson B, Heinesch B, Aubinet M (2006) Annual net ecosystem carbon exchange by a sugar beet crop. *Agricultural and Forest Meteorology* 139(1-2):25–39.
20. Aubinet M, et al. (2001) Long term carbon dioxide exchange above a mixed forest in the belgian ardennes. *Agricultural and Forest Meteorology* 108(4):293–315.
21. Miller SD, et al. (2004) Biometric and micrometeorological measurements of tropical forest carbon balance. *Ecological Applications* 14(sp4):114–126.
22. Goulden ML, et al. (2006) An eddy covariance mesonet to measure the effect of forest age on land–atmosphere exchange. *Global Change Biology* 12(11):2146–2162.
23. Bergeron O, et al. (2007) Comparison of carbon dioxide fluxes over three boreal black spruce forests in canada. *Global Change Biology* 13(1):89–107.
24. Eugster W, Zeeman MJ (2006) Micrometeorological techniques to measure ecosystem-scale greenhouse gas fluxes for model validation and improvement in *International Congress Series*. (Elsevier), Vol. 1293, pp. 66–75.
25. Ammann C, Flechard C, Leifeld J, Neftel A, Fuhrer J (2007) The carbon budget of newly established temperate grassland depends on management intensity. *Agriculture, Ecosystems & Environment* 121(1-2):5–20.
26. Zhang JH, Han SJ, Yu GR (2006) Seasonal variation in carbon dioxide exchange over a 200-year-old chinese broad-leaved korean pine mixed forest. *Agricultural and Forest Meteorology* 137(3-4):150–165.
27. Dong G, et al. (2011) Effects of spring drought on carbon sequestration, evapotranspiration and water use efficiency in the songnen meadow steppe in northeast china. *Ecohydrology* 4(2):211–224.
28. Yu GR, et al. (2006) Overview of chinaflux and evaluation of its eddy covariance measurement. *Agricultural and Forest Meteorology* 137(3-4):125–137.
29. Chen S, et al. (2009) Energy balance and partition in inner mongolia steppe ecosystems with different land use types. *Agricultural and Forest Meteorology* 149(11):1800–1809.
30. Fu YL, et al. (2006) Depression of net ecosystem co2 exchange in semi-arid leymus chinensis steppe and alpine shrub. *Agricultural and Forest Meteorology* 137(3-4):234–244.
31. Kato T, et al. (2006) Temperature and biomass influences on interannual changes in co2 exchange in an alpine meadow on the qinghai-tibetan plateau. *Global Change Biology* 12(7):1285–1298.
32. Shao P, Zeng X, Sakaguchi K, Monson RK, Zeng X (2013) Terrestrial carbon cycle: climate relations in eight cmip5 earth system models. *Journal of Climate* 26(22):8744–8764.

33. Gilmanov T, et al. (2007) Partitioning european grassland net ecosystem co2 exchange into gross primary productivity and ecosystem respiration using light response function analysis. *Agriculture, ecosystems & environment* 121(1-2):93–120.
34. Knohl A, Schulze ED, Kolle O, Buchmann N (2003) Large carbon uptake by an unmanaged 250-year-old deciduous forest in central germany. *Agricultural and Forest Meteorology* 118(3-4):151–167.
35. Ceschia E, et al. (2010) Management effects on net ecosystem carbon and ghg budgets at european crop sites. *Agriculture, Ecosystems & Environment* 139(3):363–383.
36. Zimmermann F, Plessow K, Queck R, Bernhofer C, Matschullat J (2006) Atmospheric n-and s-fluxes to a spruce forest—comparison of inferential modelling and the throughfall method. *Atmospheric Environment* 40(25):4782–4796.
37. Mauder M, et al. (2013) A strategy for quality and uncertainty assessment of long-term eddy-covariance measurements. *Agricultural and Forest Meteorology* 169:122–135.
38. Hommeltenberg J, Schmid HP, Drösler M, Werle P (2014) Can a bog drained for forestry be a stronger carbon sink than a natural bog forest? *Biogeosciences* 11(13):3477–3493.
39. GrüNwald T, Bernhofer C (2007) A decade of carbon, water and energy flux measurements of an old spruce forest at the anchor station tharandt. *Tellus B: Chemical and Physical Meteorology* 59(3):387–396.
40. Pilegaard K, Hummelshøj P, Jensen N, Chen Z (2001) Two years of continuous co2 eddy-flux measurements over a danish beech forest. *Agricultural and Forest Meteorology* 107(1):29–41.
41. Reverter BR, et al. (2010) Analyzing the major drivers of nee in a mediterranean alpine shrubland. *Biogeosciences* 7(9):2601–2611.
42. Vesala T, et al. (2005) Effect of thinning on surface fluxes in a boreal forest. *Global Biogeochemical Cycles* 19(2).
43. Loubet B, et al. (2011) Carbon, nitrogen and greenhouse gases budgets over a four years crop rotation in northern france. *Plant and Soil* 343(1-2):109.
44. Delpierre N, Berveiller D, Granda E, Dufrene E (2016) Wood phenology, not carbon input, controls the interannual variability of wood growth in a temperate oak forest. *The New phytologist* 210 2:459–70.
45. Rambal S, Joffre R, Ourcival J, Cavender-Bares J, Rocheteau A (2004) The growth respiration component in eddy co2 flux from a quercus ilex mediterranean forest. *Global Change Biology* 10(9):1460–1469.
46. Bonal D, et al. (2008) Impact of severe dry season on net ecosystem exchange in the neotropical rainforest of french guiana. *Global Change Biology* 14(8):1917–1933.
47. Vitale L, Di Tommasi P, D'Urso G, Magliulo V (2016) The response of ecosystem carbon fluxes to lai and environmental drivers in a maize crop grown in two contrasting seasons. *International Journal of Biometeorology* 60(3):411–420.
48. Sabbatini S, et al. (2016) Greenhouse gas balance of cropland conversion to bioenergy poplar short-rotation coppice. *Biogeosciences* 13(1):95–113.
49. Fares S, Loreto F (2015) Isoprenoid emissions by the mediterranean vegetation in castelporziano. *Rendiconti Lincei* 26(3):493–498.
50. Ferréa C, Zenone T, Comolli R, Seufert G (2012) Estimating heterotrophic and autotrophic soil respiration in a semi-natural forest of lombardy, italy. *Pedobiologia* 55(6):285–294.
51. Cescatti A, ZORER R (2003) Structural acclimation and radiation regime of silver fir (abies alba mill.) shoots along a light gradient. *Plant, Cell & Environment* 26(3):429–442.
52. Spano D, Duce P, Snyder RL, Zara P, Ventura A (2005) Assessment of fuel dryness index on mediterranean vegetation in *Proceedings of the 6th Symposium on Fire and Forest Meteorology, Cammore, Canada.*
53. Migliavacca M, et al. (2009) Seasonal and interannual patterns of carbon and water fluxes of a poplar plantation under peculiar eco-climatic conditions. *Agricultural and Forest Meteorology* 149(9):1460–1476.
54. Marcolla B, et al. (2005) Importance of advection in the atmospheric co2 exchanges of an alpine forest. *Agricultural and Forest Meteorology* 130(3-4):193–206.
55. Rey A, et al. (2002) Annual variation in soil respiration and its components in a coppice oak forest in central italy. *Global Change Biology* 8(9):851–866.
56. Tedeschi V, et al. (2006) Soil respiration in a mediterranean oak forest at different developmental stages after coppicing. *Global Change Biology* 12(1):110–121.
57. Matteucci M, Gruening C, Ballarin IG, Seufert G, Cescatti A (2015) Components, drivers and temporal dynamics of ecosystem respiration in a mediterranean pine forest. *Soil Biology and Biochemistry* 88:224–235.
58. Galvagno M, et al. (2013) Phenology and carbon dioxide source/sink strength of a subalpine grassland in response to an exceptionally short snow season. *Environmental Research Letters* 8(2):025008.
59. Yamazaki T, et al. (2013) A common stomatal parameter set used to simulate the energy and water balance over boreal and temperate forests. *Journal of the Meteorological Society of Japan. Ser. II* 91(3):273–285.
60. Van der Molen M, Gash J, Elbers J (2004) Sonic anemometer (co) sine response and flux measurement: Ii. the effect of introducing an angle of attack dependent calibration. *Agricultural and Forest Meteorology* 122(1-2):95–109.
61. Dolman A, Moors E, Elbers J (2002) The carbon uptake of a mid latitude pine forest growing on sandy soil. *Agricultural and Forest Meteorology* 111(3):157–170.
62. Kurbatova J, Li C, Varlagin A, Xiao X, Vygodskaya N (2008) Modeling carbon dynamics in two adjacent spruce forests with different soil conditions in russia. *Biogeosciences* 5(4):969–980.
63. Sjöström M, et al. (2009) Evaluation of satellite based indices for gross primary production estimates in a sparse savanna in the sudan. *Biogeosciences* 6(1):129–138.

64. Billesbach D, Bradford J (2016) Ameriflux us-ar1 arm usda unl osu woodward switchgrass 1, (AmeriFlux; US Department of Agriculture; University of Nebraska), Technical report.
65. Fischer ML, Billesbach DP, Berry JA, Riley WJ, Torn MS (2007) Spatiotemporal variations in growing season exchanges of co2, h2o, and sensible heat in agricultural fields of the southern great plains. *Earth Interactions* 11(17):1–21.
66. Goldstein A, et al. (2000) Effects of climate variability on the carbon dioxide, water, and sensible heat fluxes above a ponderosa pine plantation in the sierra nevada (ca). *Agricultural and Forest Meteorology* 101(2-3):113–129.
67. Urbanski S, et al. (2007) Factors controlling co2 exchange on timescales from hourly to decadal at harvard forest. *Journal of Geophysical Research: Biogeosciences* 112(G2).
68. Sulman B, Desai A, Cook B, Saliendra N, Mackay D (2009) Contrasting carbon dioxide fluxes between a drying shrub wetland in northern wisconsin, usa, and nearby forests. *Biogeosciences* 6(6):1115–1126.
69. Schmid HP, Grimmond CSB, Cropley F, Offerle B, Su HB (2000) Measurements of co2 and energy fluxes over a mixed hardwood forest in the mid-western united states. *Agricultural and Forest Meteorology* 103(4):357–374.
70. Law BE, et al. (2006) *CARBON FLUXES ACROSS REGIONS: OBSERVATIONAL CONSTRAINTS AT MULTIPLE SCALES*, eds. WU J, JONES KB, LI H, LOUCKS OL. (Springer Netherlands, Dordrecht), pp. 167–190.
71. Ruehr NK, Martin JG, Law BE (2012) Effects of water availability on carbon and water exchange in a young ponderosa pine forest: Above-and belowground responses. *Agricultural and forest meteorology* 164:136–148.
72. Sturtevant C, et al. (2016) Identifying scale-emergent, nonlinear, asynchronous processes of wetland methane exchange. *Journal of Geophysical Research: Biogeosciences* 121(1):188–204.
73. Verma SB, et al. (2005) Annual carbon dioxide exchange in irrigated and rainfed maize-based agroecosystems. *Agricultural and Forest Meteorology* 131(1-2):77–96.
74. Monson RK, et al. (2002) Carbon sequestration in a high-elevation, subalpine forest. *Global Change Biology* 8(5):459–478.
75. Desai AR, et al. (2015) Landscape-level terrestrial methane flux observed from a very tall tower. *Agricultural and Forest Meteorology* 201:61 – 75.
76. Scott RL, Biederman JA, Hamerlynck EP, Barron-Gafford GA (2015) The carbon balance pivot point of southwestern u.s. semiarid ecosystems: Insights from the 21st century drought. *Journal of Geophysical Research: Biogeosciences* 120(12):2612–2624.
77. Scott RL (2010) Using watershed water balance to evaluate the accuracy of eddy covariance evaporation measurements for three semiarid ecosystems. *Agricultural and Forest Meteorology* 150(2):219–225.
78. Desai AR, Bolstad PV, Cook BD, Davis KJ, Carey EV (2005) Comparing net ecosystem exchange of carbon dioxide between an old-growth and mature forest in the upper midwest, usa. *Agricultural and Forest Meteorology* 128(1-2):33–55.
79. Baldocchi DD, Xu L, Kiang N (2004) How plant functional-type, weather, seasonal drought, and soil physical properties alter water and energy fluxes of an oak–grass savanna and an annual grassland. *Agricultural and Forest Meteorology* 123(1-2):13–39.
80. Hatala JA, et al. (2012) Greenhouse gas (co2, ch4, h2o) fluxes from drained and flooded agricultural peatlands in the sacramento-san joaquin delta. *Agriculture, Ecosystems Environment* 150:1 – 18.
81. Rothstein DE, Zak DR, Pregitzer KS, Curtis PS (2000) Kinetics of nitrogen uptake by populus tremuloides in relation to atmospheric co2 and soil nitrogen availability. *Tree Physiology* 20(4):265–270.
82. Gough CM, et al. (2013) Sustained carbon uptake and storage following moderate disturbance in a great lakes forest. *Ecological Applications* 23(5):1202–1215.
83. Ma S, Baldocchi DD, Xu L, Hehn T (2007) Inter-annual variability in carbon dioxide exchange of an oak/grass savanna and open grassland in california. *Agricultural and Forest Meteorology* 147(3-4):157–171.
84. Cook BD, et al. (2004) Carbon exchange and venting anomalies in an upland deciduous forest in northern wisconsin, usa. *Agricultural and Forest Meteorology* 126(3-4):271–295.
85. Scott R (2016) Ameriflux us-wkg walnut gulch kendall grasslands, (AmeriFlux; United States Department of Agriculture), Technical report.
86. Scholes R, et al. (2001) The environment and vegetation of the flux measurement site near skukuza. *Koedoe* pp. 73–83.
87. Scanlon T, Albertson J (2004) Canopy scale measurements of co2 and water vapor exchange along a precipitation gradient in southern africa. *Global Change Biology* 10(3):329–341.